http://dx.doi.org/10.1016/j.cam.2015.01.042

Restricted Ornstein-Uhlenbeck process and applications in neuronal models with periodic input signals

A. Buonocore[a], L. Caputo[a], A.G. Nobile[b], E. Pirozzi[a]

[a] *Dipartimento di Matematica e Applicazioni, Università di Napoli Federico II, Monte S. Angelo, 80126, Napoli, Italy, {anibuono,luigia.caputo,epirozzi}@unina.it*
[b] *Dipartimento di Studi e Ricerche Aziendali (Management & Information Technology), Università di Salerno, Via Giovanni Paolo II, n. 132, 84084 Fisciano (SA), Italy, nobile@unisa.it*

Abstract

Restricted Gauss-Markov processes are used to construct inhomogeneous leaky integrate-and-fire stochastic models for single neurons activity in the presence of a lower reflecting boundary and periodic input signals. The first-passage time problem through a time-dependent threshold is explicitly developed; numerical, simulation and asymptotic results for firing densities are provided.

Keywords: Gauss-Markov processes, Integrate-and-fire model, Firing densities, Volterra integral equations, Asymptotic behavior, Simulation
2010 MSC: 60G15, 60J60, 92C20, 65C30

1. Introduction

One-dimensional continuous-time Markov processes have been widely invoked as models to account for statistical features of spike trains recorded from single neurons belonging to complex networks (cf. [10], [26], [35]). Among these, the leaky integrate-and-fire (LIF) neuronal models, based on unrestricted Ornstein-Uhlenbeck processes, play a relevant role to describe the stochastic fluctuations in the membrane potential of a neuron. In order to analyze the statistical properties of the interspike intervals in the LIF neuronal model, the first-passage time (FPT) of the unrestricted Ornstein-Uhlenbeck process through time-dependent firing thresholds has been extensively studied by means of numerical procedures, simulation algorithms and asymptotic methods (cf. for instance, [1], [6], [31], [33], [34] and references therein). Particular attention has been dedicated to investigate the behavior of the stochastic LIF model when an additional periodic input in the drift is introduced (cf., for instance, [4], [7], [13], [14], [18], [20], [27], [32]). In such a context it is shown that the periodicity of the input signal produces an oscillatory behavior of the firing probability density function (pdf), leading to a multimodal FPT pdf (see [2], [9], [22], [28], [30]).

In order to embody additional physiological features of real neurons, several alternative models have been proposed that take into account the existence of

the reversal potential, which restricts the state space of the continuous stochastic process from below (cf., for instance, [15], [16], [17], [21]). One possibility is to describe the evolution of the membrane potential by focusing the attention on stochastic processes restricted by a reflecting boundary that can be looked at as the neuronal reversal hyperpolarization potential.

In the present paper, inhomogeneous stochastic LIF models for single neurons activity in the presence of a reflecting boundary and periodic input signals are analyzed. In particular, making use of results obtained in [5], in Section 2 restricted inhomogeneous LIF stochastic models with time-varying input signals are considered, such that the transition pdf admits a closed form expression. The knowledge of the transition pdf allows to obtain the FPT pdf through a time-dependent firing threshold by using suitable numerical methods and appropriate simulation algorithms. In Section 3, for the restricted inhomogeneous LIF stochastic model, we specialize the results obtained in [5] to the case of periodic input signals; furthermore, the asymptotic behavior of the transition pdf is determined. In Section 4, the firing densities for the unrestricted LIF process and for the restricted LIF process with periodic input signal are compared by using numerical and simulation procedures, showing that the FPT densities may exhibit damped oscillations having the same period of the periodic input signal. Finally, when the threshold is progressively moved away from the starting point of the related processes, non-homogeneous exponential approximations are shown to hold for the firing densities.

2. Time non-homogeneous stochastic LIF model

We consider the Gauss-Markov process $\{Y(t), t \geq 0\}$, characterized by the mean function

$$m(t) = \varrho\left(1 - e^{-t/\vartheta}\right) + \int_0^t \mu(\xi)\, e^{-(t-\xi)/\vartheta}\, d\xi \qquad (t \geq 0), \tag{1}$$

and the covariance function $c(s,t) = h_1(s)\, h_2(t)$ $(0 \leq s \leq t)$ such that

$$h_1(t) = e^{t/\vartheta} \int_0^t \sigma^2(\xi)\, e^{-2\,(t-\xi)/\vartheta}\, d\xi, \quad h_2(t) = e^{-t/\vartheta} \qquad (t \geq 0), \tag{2}$$

where $\vartheta > 0$, $\varrho \in \mathbb{R}$ and $\mu(t), \sigma(t) \in C^1(0, +\infty)$, with $\sigma(t) > 0$. The transition density $f_Y(x,t|y,\tau)$ is a normal pdf with the following mean and variance:

$$M(t|y,\tau) = y\, e^{-(t-\tau)/\vartheta} + \varrho\left(1 - e^{-(t-\tau)/\vartheta}\right) + \int_\tau^t \mu(\xi)\, e^{-(t-\xi)/\vartheta}\, d\xi, \qquad (0 \leq \tau \leq t) \tag{3}$$

$$V(t|\tau) = \int_\tau^t \sigma^2(\xi)\, e^{-2\,(t-\xi)/\vartheta}\, d\xi.$$

The infinitesimal moments of $Y(t)$ are

$$A_1(x,t) = -\frac{x-\varrho}{\vartheta} + \mu(t), \qquad A_2(t) = \sigma^2(t) \qquad (x \in \mathbb{R}, \vartheta > 0, \varrho \in \mathbb{R}), \tag{4}$$

that identify the drift and the infinitesimal variance of a time non-homogeneous Ornstein-Uhlenbeck process, whose state space is the interval $(-\infty, +\infty)$; such a process is solution of the stochastic differential equation:

$$dY(t) = -\Big\{\frac{Y(t)-\varrho}{\vartheta} - \mu(t)\Big\}\, dt + \sigma(t)\, dW(t), \qquad Y(\tau) = y \tag{5}$$

where $W(t)$ denotes the standard Brownian motion. In the context of neuronal models, (4) and (5) characterize an inhomogeneous LIF diffusion process $Y(t)$, describing the evolution of the membrane potential (cf., for instance, [7] and references therein). The time constant ϑ governs the spontaneous decay of the membrane potential to the resting level ϱ, the function $\mu(t)$ represents deterministic input signal to the neuron, whereas the infinitesimal variance $\sigma^2(t)$ gives the intensity of the noise.

For the process $Y(t)$ we assume that neural firing takes place, and consequently an action potential (spike) is observed whenever the neuron's membrane potential $Y(t)$ reaches the firing threshold $S(t)$. To this purpose, let $S(t)$ be a $C^1(0,+\infty)$-class function and denote by $g_Y[S(t),t|y,\tau]$ the FPT pdf of $Y(t)$ from $Y(\tau)=y$ to the firing threshold $S(t)$. As shown in [3], [8], [11] the FPT pdf $g_Y[S(t),t|y,\tau]$ satisfies a non-singular second-kind Volterra integral equation

$$g_Y[S(t),t|y,\tau] = -2\Psi_Y[S(t),t|y,\tau] + 2\int_\tau^t g_Y[S(u),u|y,\tau]\Psi_Y[S(t),t|S(u),u]\, du \qquad \big[y < S(\tau)\big], \tag{6}$$

where

$$\Psi_Y[S(t),t|y,\tau] = \Bigg\{\frac{S'(t)-m'(t)}{2} + \frac{S(t)-m(t)}{2}\left[\frac{1}{\vartheta} - \frac{\sigma^2(t)e^{2t/\vartheta}}{\int_\tau^t \sigma^2(\xi)\, e^{2\xi/\vartheta}\, d\xi}\right] + \frac{y-m(\tau)}{2}\frac{\sigma^2(t)e^{(t+\tau)/\vartheta}}{\int_\tau^t \sigma^2(\xi)\, e^{2\xi/\vartheta}\, d\xi}\Bigg\} f_Y[S(t),t|y,\tau], \tag{7}$$

and $f_Y(x,t|y,\tau)$ is the transition pdf of $Y(t)$.

In the neuronal model (4) the state space for the underlying stochastic process is the entire real axis, that is arbitrarily large hyperpolarization values for the membrane potential are possible. Some authors (see, for instance, [16], [17], [21]) have suggested alternative models by assuming the existence of a lower boundary for the membrane potential. For this reason, in [5] we focused on the stochastic process $\{X(t), t \geq 0\}$, with state space $[\nu(t), +\infty)$, obtained by considering $\{Y(t), t \geq 0\}$ in the presence of the following reflecting lower boundary

$$\nu(t) = \varrho\,(1 - e^{-t/\vartheta}) + \int_0^t \mu(\xi)\, e^{-(t-\xi)/\vartheta} d\xi + B\, e^{-t/\vartheta}, \tag{8}$$

where the real constant B is chosen in order to ensure that the starting point of the process $X(t)$ is greater or equal to the reflecting boundary at the initial time, i.e. $y \geq \nu(\tau)$. We note that the choice of the reflecting boundary (8) is

motivated by the need to obtain a closed-form expression for the transition pdf of the process $X(t)$ in the case of time-dependent input signal. On the other hand, by choosing $B = \nu \leq y$ and $\mu(t) = -(\varrho - \nu)/\vartheta$ in (8), the reflecting lower boundary $\nu(t)$ is identified with the constant ν.

As proved in [5] the transition pdf of the stochastic process $\{X(t), t \geq 0\}$, obtained by considering $Y(t)$ in presence of the reflecting boundary $\nu(t)$, is:

$$f_X(x,t|y,\tau) = f_Y(x,t|y,\tau) + f_Y[2\,\nu(t) - x, t|y,\tau] \qquad \big[x \geq \nu(t),\ y \geq \nu(\tau)\big], \tag{9}$$

where $f_Y(x,t|y,\tau)$ is the transition pdf of $Y(t)$, with mean and variance given in (3). We note that the expression of the reflecting boundary (8) is not affected by the intensity of the noise $\sigma^2(t)$, which instead always plays a fundamental role in the transition pdf (9).

For the process $X(t)$, restricted in $[\nu(t), +\infty)$ with the reflecting boundary $\nu(t)$ given in (8), let $S(t)$ be a $C^1(0,+\infty)$-class function, such that $S(t) > \nu(t)$ for all $t \geq 0$ and denote by $g_X[S(t),t|y,\tau]$ the FPT pdf of $X(t)$ from $X(\tau) = y \geq \nu(\tau)$ to the firing threshold $S(t)$. As proved in [5], the FPT pdf $g_X[S(t),t|y,\tau]$ satisfies a non-singular second-kind Volterra integral equation

$$g_X[S(t),t|y,\tau] = -2\Psi_X[S(t),t|y,\tau] + 2\int_\tau^t g_X[S(u),u|y,\tau]\Psi_X[S(t),t|S(u),u]\,du \qquad \big[\nu(\tau) \leq y < S(\tau)\big] \tag{10}$$

where

$$\begin{aligned}\Psi_X[S(t),t|y,\tau] = \Bigg\{ &\frac{S'(t) - m'(t)}{2} + \frac{S(t) - m(t)}{2}\left[\frac{1}{\vartheta} - \frac{\sigma^2(t)e^{2t/\vartheta}}{\int_\tau^t \sigma^2(\xi)\,e^{2\xi/\vartheta}\,d\xi}\right] \\ &+ \frac{y - m(\tau)}{2}\frac{\sigma^2(t)e^{(t+\tau)/\vartheta}}{\int_\tau^t \sigma^2(\xi)\,e^{2\xi/\vartheta}\,d\xi}\Bigg\} f_X[S(t),t|y,\tau] \\ &- \frac{[y - \nu(\tau)]\,\sigma^2(t)e^{(t+\tau)/\vartheta}}{\int_\tau^t \sigma^2(\xi)\,e^{2\xi/\vartheta}\,d\xi}\, f_Y[2\,\nu(t) - S(t),t|y,\tau],\end{aligned} \tag{11}$$

with $\nu(t)$ given in (8) and where $f_X(x,t|y,\tau)$ and $f_Y(x,t|y,\tau)$ are the transition pdfs of $X(t)$ and $Y(t)$, respectively.

For $k = 1, 2, \ldots$ we denote by

$$\begin{aligned} t_k^{(Y)}(y,\tau) &:= \int_\tau^{+\infty} t^k g_Y[S(t),t|y,\tau]\,dt \qquad [y < S(\tau)], \\ t_k^{(X)}(y,\tau) &:= \int_\tau^{+\infty} t^k g_X[S(t),t|y,\tau]\,dt \qquad \big[\nu(\tau) \leq y < S(\tau)\big], \end{aligned} \tag{12}$$

the k–order moments of the FPT for the unrestricted LIF process $Y(t)$ and for the restricted LIF process $X(t)$, respectively; furthermore, $\mathrm{Var}^{(Y)}(y,\tau) = t_2^{(Y)}(y,\tau) - [t_1^{(Y)}(y,\tau)]^2$ and $\mathrm{Var}^{(X)}(y,\tau) = t_2^{(X)}(y,\tau) - [t_1^{(X)}(y,\tau)]^2$ indicate the

variances of FPT for $Y(t)$ and $X(t)$, respectively. Moreover, with $\Sigma^{(Y)}(y,\tau)$ and $\Sigma^{(X)}(y,\tau)$ we denote the skewness of the FPT for $Y(t)$ and $X(t)$, respectively. The skewness, evaluated as $\Sigma = [t_3 + 2t_1^3 - 3t_1 t_2]/[t_2 - t_1^2]^{3/2}$, gives a measure of the degree of asymmetry of the FTP density.

In the next sections we specialize the above results to the case of restricted LIF neuronal models in which the input signal is a periodic function of time and the threshold is constant.

3. Neuronal model with periodic input signals

We now suppose that the input signal $\mu(t)$ in (1) is the periodic function

$$\mu(t) = \mu + \lambda \cos(\omega\, t + \phi) \qquad (\lambda \neq 0, \phi \in \mathbb{R}, \omega > 0) \tag{13}$$

for $t \geq 0$, whose period is $Q = 2\pi/\omega$. The periodic input signal (13) oscillates around the constant μ with angular frequency ω, initial phase ϕ and input amplitude λ. Making use of (13) in (1) one has

$$m(t) = (\varrho + \mu\,\vartheta)\,(1 - e^{-t/\vartheta}) + \frac{\lambda\,\vartheta}{1 + \omega^2\,\vartheta^2}\Big\{\cos(\omega\, t + \phi) + \omega\,\vartheta \sin(\omega\, t + \phi) - \big[\cos\phi + \omega\,\vartheta\, \sin\phi\big]\, e^{-t/\vartheta}\Big\} \qquad (t \geq 0). \tag{14}$$

Hence, we consider the Gauss-Markov process $\{Y(t), t \geq 0\}$ with mean function (14) and covariance factors given in (2). The infinitesimal moments of $Y(t)$ are given in (4) with $\mu(t)$ as in (13). The conditional mean of $Y(t)$ follows from (3):

$$M(t|y,\tau) = y\, e^{-(t-\tau)/\vartheta} + (\varrho + \mu\,\vartheta)\,[1 - e^{-(t-\tau)/\vartheta}] + \frac{\lambda\,\vartheta}{1 + \omega^2\,\vartheta^2}\Big\{\cos(\omega\, t + \phi) + \omega\,\vartheta \sin(\omega\, t + \phi) - \big[\cos(\omega\,\tau + \phi) + \omega\,\vartheta\, \sin(\omega\,\tau + \phi)\big]\, e^{-(t-\tau)/\vartheta}\Big\} \qquad (0 \leq \tau \leq t). \tag{15}$$

In the absence of noise, i.e. $\sigma(t) = 0$, the mean $M(t|y,\tau)$ coincides with the solution of the deterministic version of (5) with $\mu(t)$ as in (13). Furthermore, from (14) and (15) one obtains the asymptotic behavior of the conditional mean:

$$\widetilde{M}(t) = \lim_{n\to+\infty} M(t + n\,Q|y,\tau) \equiv \lim_{n\to+\infty} m(t + n\,Q) = \varrho + \mu\,\vartheta + \frac{\lambda\,\vartheta}{1 + \omega^2\vartheta^2}\Big\{\cos(\omega\, t + \phi) + \omega\,\vartheta \sin(\omega\, t + \phi)\Big\}. \tag{16}$$

Note that $\widetilde{M}(t)$ is a periodic function of period $Q = 2\pi/\omega$ and its average in a period is:

$$m_{\scriptscriptstyle P} = \frac{1}{Q}\int_0^Q \widetilde{M}(t)\, dt = \varrho + \mu\,\vartheta. \tag{17}$$

When the firing threshold is constant, i.e $S(t) = S$, in the absence of noise one can distinguish between subthreshold and suprathreshold regimes. If

$$m_\infty \equiv \sup_{t\geq 0} \widetilde{M}(t) = \varrho + \mu\,\vartheta + \frac{|\lambda|\,\vartheta}{\sqrt{1+\omega^2\vartheta^2}} \tag{18}$$

takes values larger than S, then LIF generates sustained firing. If, conversely, m_∞ remains below the constant threshold S, then the LIF will fire at most a finite number of discharges and remain quiescent henceforth. Therefore, stimuli are classified as subthreshold if $m_\infty \leq S$ and suprathreshold otherwise (cf. [24], [25], [29]).

In the remaining part of the paper we consider the process $\{X(t), t \geq 0\}$, obtained by confining $Y(t)$ to the interval $[\nu(t), +\infty)$ with the reflecting boundary

$$\begin{aligned}\nu(t) = (\varrho + \mu\,\vartheta)\,(1 - e^{-t/\vartheta}) + \frac{\lambda\,\vartheta}{1+\omega^2\,\vartheta^2}\Big\{&\cos(\omega\,t+\phi) + \omega\,\vartheta\sin(\omega\,t+\phi)\\ &-\big[\cos\phi + \omega\,\vartheta\sin\phi\big]\,e^{-t/\vartheta}\Big\} + B\,e^{-t/\vartheta} \qquad (B\in\mathbb{R}),\end{aligned} \tag{19}$$

obtained from (8) by using (13). By virtue of (9), for $y \geq \nu(\tau)$ the conditional mean and the second order conditional moment of $X(t)$ are:

$$\begin{aligned}E[X(t)|X(\tau)=y] := \int_{\nu(t)}^{+\infty} x\,f_X(x,t|y,\tau)\,dx &= \sqrt{\frac{2V(t|\tau)}{\pi}}\,e^{-H^2(t|y,\tau)}\\ &+\frac{1}{2}\,M(t|y,\tau)\Big\{1+\mathrm{Erf}\big[H(t|y,\tau)\big]\Big\}\\ &+\frac{1}{2}\Big[2\nu(t)-M(t|y,\tau)\Big]\Big\{1-\mathrm{Erf}\big[H(t|y,\tau)\big]\Big\},\end{aligned} \tag{20}$$

$$\begin{aligned}E[X^2(t)|X(\tau)=y] := \int_{\nu(t)}^{+\infty} x^2\,f_X(x,t|y,\tau)\,dx = V(t|\tau) + M^2(t|y,\tau)\\ -2\nu(t)\Big[M(t|y,\tau)-\nu(t)\Big]\Big\{1-\mathrm{Erf}\big[H(t|y,\tau)\big]\Big\} + 4\,\nu(t)\sqrt{\frac{V(t|\tau)}{2\pi}}\,e^{-H^2(t|y,\tau)},\end{aligned}$$

with $V(t|\tau)$ and $M(t|y,\tau)$ given in (3) and (15), and where we have set:

$$H(t|y,\tau) = \frac{M(t|y,\tau)-\nu(t)}{\sqrt{2V(t|\tau)}}\cdot \tag{21}$$

Differently from the LIF model, the conditional mean (20) of the process $X(t)$ is strongly influenced by the intensity of the noise, involved in the function $V(t|\tau)$.

3.1. Behavior of the lower boundary

The function $\nu(t)$ in (19) is the sum of two components $\nu_1(t)$ and $\nu_2(t)$:

$$\begin{aligned}\nu_1(t) &= \frac{\lambda\,\vartheta}{1+\omega^2\,\vartheta^2}\Big\{\cos(\omega\,t+\phi) + \omega\,\vartheta\sin(\omega\,t+\phi)\Big\},\\ \nu_2(t) &= \varrho + \mu\,\vartheta - e^{-t/\vartheta}\Big\{\varrho + \mu\,\vartheta + \frac{\lambda\,\vartheta}{1+\omega^2\,\vartheta^2}\big[\cos\phi + \omega\,\vartheta\sin\phi\big] - B\Big\}.\end{aligned} \tag{22}$$

The function $\nu_1(t)$ is a periodic function of period $Q = 2\pi/\omega$, whereas $\nu_2(t)$ is a monotonic function of t. The values of parameters $\mu, \vartheta, \varrho, \omega, \phi, B$ determine three different behaviors of $\nu(t)$:

- if $B < \varrho + \mu\,\vartheta + \dfrac{\lambda\,\vartheta}{1+\omega^2\,\vartheta^2}\big[\cos\phi + \omega\,\vartheta\sin\phi\big]$, then the function $\nu(t)$ oscillates around the *increasing* function $\nu_2(t)$;
- if $B > \varrho + \mu\,\vartheta + \dfrac{\lambda\,\vartheta}{1+\omega^2\,\vartheta^2}\big[\cos\phi + \omega\,\vartheta\sin\phi\big]$, then the function $\nu(t)$ oscillates around the *decreasing* function $\nu_2(t)$;
- if $B = \varrho + \mu\,\vartheta + \dfrac{\lambda\,\vartheta}{1+\omega^2\,\vartheta^2}\big[\cos\phi + \omega\,\vartheta\sin\phi\big]$, then the function $\nu(t)$ oscillates around the *constant* function $\nu_2(t)$.

The amplitude and the frequency of oscillations depend on the function $\nu_1(t)$. In Figure 1 the boundary $\nu(t)$ and the function $\nu_2(t)$ are plotted for $\phi = 0$ (on the left) and $\phi = 5$ (on the right). From (19) it follows that $\nu(0) = B$.

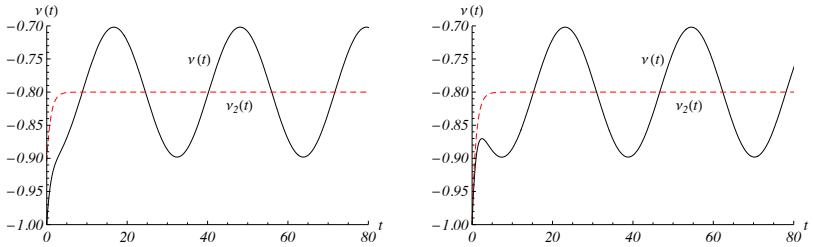

(a) $\phi = 0$ (b) $\phi = 5$

Figure 1: The boundary $\nu(t)$ (solid curve) and the function $\nu_2(t)$ (dashed curve) are plotted for $\vartheta = 1$, $\mu = 0.1$, $\varrho = -0.9$, $\lambda = -0.1$, $\omega = 0.2$ and $B = -1$.

Furthermore, denoting by

$$\xi(t) = \frac{\lambda\,\vartheta}{1+\omega^2\,\vartheta^2}\Big\{\cos(\omega\,t+\phi) + \omega\,\vartheta\sin(\omega\,t+\phi) - \big[\cos\phi + \omega\,\vartheta\sin\phi\big]\,e^{-t/\vartheta}\Big\}, \quad (23)$$

from (19) one has

$$\nu(t) = (\varrho + \mu\,\vartheta)\,(1 - e^{-t/\vartheta}) + B\,e^{-t/\vartheta} + \xi(t). \quad (24)$$

As shown in Figure 2, $\xi(t)$ becomes a periodic function starting from rather small times, with oscillations around the zero state. Furthermore, $\nu(t)$ admits an asymptotic periodic behavior:

$$\widetilde{\nu}(t) = \lim_{n\to+\infty} \nu(t + n\,Q) = \varrho + \mu\,\vartheta + \frac{\lambda\,\vartheta}{1+\omega^2\vartheta^2}\Big\{\cos(\omega\,t+\phi) + \omega\,\vartheta\,\sin(\omega\,t+\phi)\Big\}, \quad (25)$$

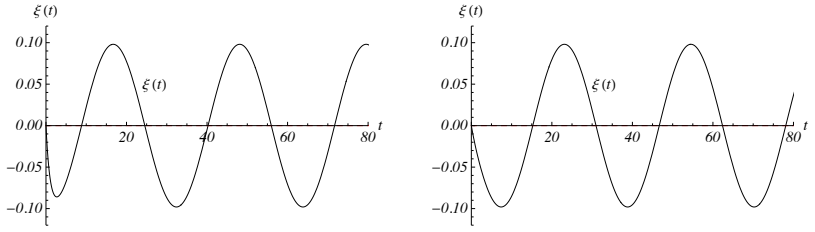

(a) $\phi = 0$ (b) $\phi = 5$

Figure 2: The function $\xi(t)$ is plotted for the same choices of the parameters of Figure 1.

that identifies with $\widetilde{M}(t)$, given in (16). We note that the asymptotic average of $\widetilde{\nu}(t)$ in a period is:

$$\nu_{\scriptscriptstyle P} = \frac{1}{Q}\int_0^Q \widetilde{\nu}(t)\,dt = \varrho + \mu\,\vartheta, \tag{26}$$

that coincides with $m_{\scriptscriptstyle P}$, given in (17).

3.2. Asymptotic behavior of the transition pdf

We now assume that $\sigma^2(t)$ is a bounded function, such that $\lim_{n\to+\infty}\sigma^2(t+n\,Q) = \widetilde{\sigma}^2(t)$, where $\widetilde{\sigma}^2(t)$ is a constant function or a periodic function of the same period $Q = 2\pi/\omega$ of the input signal (13). Under such assumption, from the second of (3) it follows:

$$\widetilde{V}(t) = \lim_{n\to+\infty} V(t+n\,Q|\tau) = \frac{\vartheta\,\widetilde{\sigma}^2(t)}{2}\cdot \tag{27}$$

Hence, the pdf $f_X(x,t|y,\tau)$, given in (9), admits a quasi-stationary behavior as indicated in the following proposition.

Proposition 3.1. *Let $m(t)$ given in (14) and let $\sigma^2(t)$ be a bounded $C^1(0,+\infty)$-class function, such that $\lim_{n\to+\infty}\sigma^2(t+n\,Q) = \widetilde{\sigma}^2(t)$, where $\widetilde{\sigma}^2(t)$ is a constant function or a periodic function of period $Q = 2\pi/\omega$. Then, $X(t)$ admits the quasi-stationary density:*

$$W_X(x,t) = \lim_{n\to+\infty} f_X(x,t+nQ|y,\tau) = \frac{2}{\widetilde{\sigma}(t)\sqrt{\pi\vartheta}}\,\exp\Big\{-\frac{\big[x-\widetilde{\nu}(t)\big]^2}{\vartheta\,\widetilde{\sigma}^2(t)}\Big\} \quad [x \geq \widetilde{\nu}(t)]. \tag{28}$$

Furthermore, the first two conditional moments and the variance of $X(t)$ admit the quasi-stationary asymptotic behaviors:

$$\begin{aligned} \widetilde{M}_X(t) &= \lim_{n\to+\infty} E[X(t+n\,Q)|X(\tau)=y] = \widetilde{\nu}(t) + \widetilde{\sigma}(t)\,\sqrt{\frac{\vartheta}{\pi}}, \\ \widetilde{V}_X(t) &= \lim_{n\to+\infty} \mathrm{Var}[X(t+n\,Q)|X(\tau)=y] = \vartheta\,\widetilde{\sigma}^2(t)\,\Big(\frac{1}{2}-\frac{1}{\pi}\Big). \end{aligned} \tag{29}$$

Proof. Making use of (16), (25) and (27), expression (28) follows from (9). Furthermore, recalling that $y > \nu(\tau)$, from (21) one has:

$$\lim_{n\to+\infty} H(t+n\,Q|y,\tau) = \lim_{n\to+\infty} \frac{M(t+n\,Q|y,\tau) - \nu(t+n\,Q)}{\sqrt{2V(t+n\,Q|\tau)}} = 0,$$

so that from (20) one obtains (29). □

We note that $\widetilde{M}(t) = \widetilde{\nu}(t)$ for the unrestricted Ornstein-Uhlenbeck process $Y(t)$, whereas $\widetilde{M}_X(t) > \widetilde{\nu}(t)$ for the restricted Ornstein-Uhlenbeck process $X(t)$. Furthermore, by comparing the asymptotic means and variances of $X(t)$ and $Y(t)$, one has $\widetilde{M}_X(t) > \widetilde{M}(t)$ and $\widetilde{V}_X(t) < \widetilde{V}(t)$.

Proposition 3.1 also implies that when $\widetilde{\sigma}^2(t)$ is a constant function, the asymptotic boundary $\widetilde{\nu}(t)$ and the asymptotic conditional mean $\widetilde{M}_X(t)$ are periodic functions with the same period and with the same amplitude. Instead, when $\widetilde{\sigma}^2(t)$ is a periodic function of period $Q = 2\pi/\omega$, the asymptotic boundary $\widetilde{\nu}(t)$ and the asymptotic conditional mean are periodic functions with the same period, but the amplitudes of oscillations can be not equal. This suggests the importance of the choice of a periodic infinitesimal variance in the non-stationary Ornstein-Uhlenbeck neuronal model with the periodic signal (13) and the reflecting boundary (19). For instance, for $\mu(t)$ as in (13), the cases $\sigma^2(t) = \sigma^2$ and $\sigma^2(t) = \sigma^2\big(1 - e^{-2t/\vartheta}\big)^2$ admit the same quasi-stationary density (28), with $\widetilde{\sigma}^2(t) = \sigma^2$ and $\widetilde{\nu}(t)$ given in (25).

Under the assumption of Proposition 3.1, denoting by

$$\sigma_{\scriptscriptstyle P} = \frac{1}{Q}\int_0^Q \widetilde{\sigma}(t)\,dt, \tag{30}$$

the asymptotic average of $\widetilde{\sigma}(t)$ in a period , from (29) we obtain

$$M_{\scriptscriptstyle P} = \frac{1}{Q}\int_0^Q \widetilde{M}_X(t)\,dt = \nu_{\scriptscriptstyle P} + \sqrt{\frac{\vartheta}{\pi}}\left\{\frac{1}{Q}\int_0^Q \widetilde{\sigma}(t)\,dt\right\} = \varrho + \mu\,\vartheta + \sqrt{\frac{\vartheta}{\pi}}\,\sigma_{\scriptscriptstyle P}, \tag{31}$$

which can be interpreted as the asymptotic average of $\widetilde{M}_X(t)$ in a period.

When the firing threshold and the intensity of noise are constant, i.e $S(t) = S$ and $\sigma^2(t) = \sigma^2$, for the process $X(t)$ one can distinguish between subthreshold and suprathreshold regimes. Indeed, taking into account only the asymptotic mean, we denote by

$$M_\infty \equiv \sup_{t\geq 0} \widetilde{M}_X(t) = \varrho + \mu\,\vartheta + \frac{|\lambda|\,\vartheta}{\sqrt{1+\omega^2\vartheta^2}} + \sqrt{\frac{\vartheta}{\pi}}\,\sigma = m_\infty + \sqrt{\frac{\vartheta}{\pi}}\,\sigma, \tag{32}$$

with m_∞ given in (18). By comparing (18) and (32) we note that for the restricted process $X(t)$, M_∞ depends on the noise intensity, so that the concept of subthreshold and suprathreshold is changed with respect to that of the

LIF process $Y(t)$. In analogy to the unrestricted LIF process $Y(t)$, for the restricted process $X(t)$ stimuli can be classified as subthreshold if $M_\infty \leq S$ and suprathreshold otherwise. Therefore, the behavior of the restricted neuronal model $X(t)$ is more affected by the variability of the noise intensity.

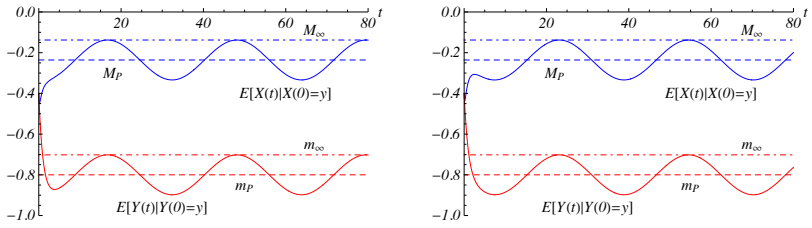

(a) $\phi = 0$ (b) $\phi = 5$

Figure 3: For the processes $Y(t)$ and $X(t)$, the conditional means $E[Y(t)|Y(0) = y]$ and $E[X(t)|X(0) = y]$ are plotted for $\vartheta = 1$, $\mu = 0.1$, $\varrho = -0.9$, $\lambda = -0.1$, $\omega = 0.2$, $\sigma^2 = 1$, $B = -1$ and $y = -0.4$. The dashed lines indicate the related asymptotic averages in a period and the dot-dashed lines indicate the upper bound of the asymptotic averages.

Figure 3 shows the conditional means $E[Y(t)|Y(0) = y]$ and $E[X(t)|X(0) = y]$ for the unrestricted Ornstein-Uhlenbeck process $Y(t)$ and for the restricted process $X(t)$ for $\sigma^2(t) \equiv \sigma^2$ constant. The dashed lines indicate the related asymptotic averages in a period, with $\sigma_P = \sigma$, whereas the dot-dashed lines indicate the upper bound of the asymptotic averages. Taking in account the choices of parameters of Figure 3, from (17), (18), (31) and (32) for the process $Y(t)$ we obtain $m_P = \varrho + \mu\,\theta = -0.8$, $m_\infty = -0.701942$, whereas for the process $X(t)$ results $M_P = m_P + 1/\sqrt{\pi} = -0.23581$ and $M_\infty = -0.137752$.

4. Firing density

For the process $X(t)$ with transition pdf (9) and subject to the periodic input signal (13), we analyze the behavior of the firing pdf $g[S(t), t|y, \tau]$ by means of numerical, simulation and asymptotic methods. Moreover, we compare the firing densities of the unrestricted process $Y(t)$ and of the restricted process $X(t)$. The firing pdf $g_Y[S(t), t|y, \tau]$ satisfies (6) with $\Psi_Y[S(t), t|y, \tau]$ given in (7), whereas $g_X[S(t), t|y, \tau]$ is solution of (10) with $\Psi_X[S(t), t|y, \tau]$ given in (11). The firing densities $g_Y[S(t), t|y, \tau]$ and $g_X[S(t), t|y, \tau]$ are obtained making use of the numerical algorithm proposed in [8]. It should be emphasized that the analysis of the FPT densities plays an important role when the input signal is reset to some fixed value after each firing and the process starts again at the initial time. In this case all interspike interval lengths are statistically independent, identically distributed random variables and the series of interspike intervals generate a renewal process.

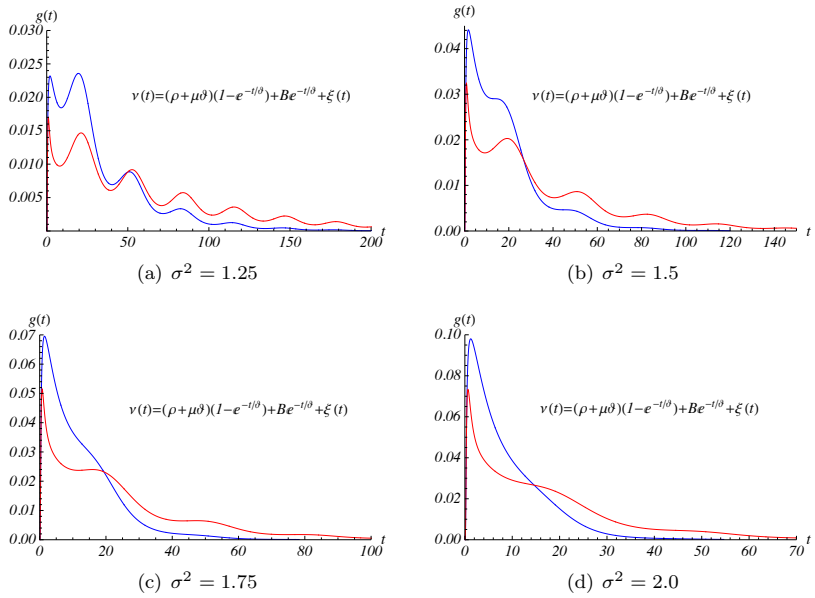

(a) $\sigma^2 = 1.25$ (b) $\sigma^2 = 1.5$

(c) $\sigma^2 = 1.75$ (d) $\sigma^2 = 2.0$

Figure 4: For the periodic input signal (13), $g_Y(S,t|y,\tau)$ (red curve) and $g_X(S,t|y,\tau)$ (blue curve) are plotted for $\vartheta = 1$, $\mu = 0.1$, $\varrho = -0.9$, $\lambda = -0.1$, $\omega = 0.2$, $\phi = 5$, $B = -1$, $\tau = 0$, $y = -0.4$ and $S = 1.5$.

4.1. Influence of the noise and of the periodic input signal

For the case of the periodic input signal (13), in Figures 4 and 5 we plot the firing pdf $g_Y(S,t|y,0)$ of the unrestricted process $Y(t)$ (red curve) and the firing pdf $g_X(S,t|y,0)$ of $X(t)$ (blue curve) through the constant threshold $S = 1.5$, starting from the initial state $y = -0.4$ at time $\tau = 0$; all cases considered are related to a subthreshold regime. The integration step in the numerical algorithm is set at 0.05. In particular, Figure 4 shows that low noise intensities bring out many peaks; furthermore, when the noise intensity increases the firing densities are concentrated into the first peaks. Figure 5 shows similar results as in Figure 4, except that the amplitude $|\lambda|$ of the input signal is increased. By comparing Figures 4 and 5 for low noise intensities, we note that the peaks of the firing densities become more visible when the amplitude $|\lambda|$ of the input signal increases; furthermore, when the intensity of the noise increases, the amplitude $|\lambda|$ of the input signal does not affect essentially in the shape of the firing densities.

Making use of the computed firing densities $g_Y[S(t),t|y,\tau]$ and $g_X[S(t),t|y,\tau]$, obtained by solving the integral equations (6) and (10), the FPT moments (12) can be numerically obtained. For the cases considered in Figures 4 and 5, with periodic input signal (13), in Table 1 we compare the mean $t_1^{(Y)}(y,\tau)$, the variance $\mathrm{Var}^{(Y)}(y,\tau)$ and the skewness $\Sigma^{(Y)}(y,\tau)$ of the FPT for the unrestricted

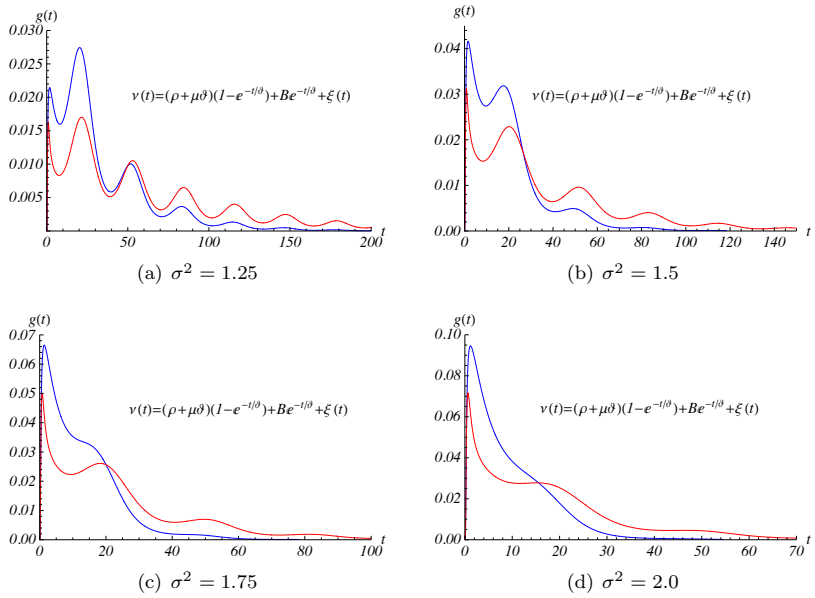

(a) $\sigma^2 = 1.25$ (b) $\sigma^2 = 1.5$

(c) $\sigma^2 = 1.75$ (d) $\sigma^2 = 2.0$

Figure 5: As in Figure 4 with $\lambda = -0.15$.

LIF process $Y(t)$ with $t_1^{(X)}(y,\tau)$, $\mathrm{Var}^{(X)}(y,\tau)$ and $\Sigma^{(X)}(y,\tau)$ of the restricted LIF process $X(t)$, respectively. We note that the mean of FPT for the restricted process is approximately halved compared to that of the unrestricted process, whereas the variance of FPT for the process $X(t)$ is about a quarter compared to that of the process $Y(t)$. Furthermore, the FPT skewness is less than 2 for both the processes $Y(t)$ and $X(t)$, implying that an exponential asymptotic regime is not yet reached.

For the case of the periodic input signal (13) with the noise intensity function $\sigma^2(t) = \sigma^2(1 - e^{-2t/\vartheta})^2$, in Figure 6 we plot the firing pdf $g_Y(S,t|y,0)$ of the unrestricted process $Y(t)$ (red curve) and the firing pdf $g_X(S,t|y,0)$ of $X(t)$ (blue curve) through the constant threshold $S = 1.5$, starting from the initial state $y = -0.4$ at time $\tau = 0$. The integration step in the numerical algorithm is again set at 0.05. By comparing Figure 4(a) with Figure 6(a) and Figure 5(a) with Figure 6(b), we note that the second peaks of the firing densities of Figure 6 are now more pronounced for both the processes $Y(t)$ and $X(t)$.

In Figure 7 we assume $\sigma^2(t) = \sigma^2 = 1$. We note that for low intensity of the noise, the firing densities contain a series of peaks spaced by multiples of the period $Q = 2\pi/\omega$ of the input signal. The location of the first peak depends on the phase ϕ, while subsequent peaks are strongly influenced on the frequency of the periodic input. Differently from Figure 4, the firing densities of Figure 7 have many peaks and the height of the peaks decreases exponentially. Moreover, the firing densities $g_Y(S,t|y,0)$ and $g_X(S,t|y,0)$ in Figure 7 exhibit damped os-

		Unrestricted process $Y(t)$			Restricted process $X(t)$		
λ	σ^2	$t_1^{(Y)}$	$\mathrm{Var}^{(Y)}$	$\Sigma^{(Y)}$	$t_1^{(X)}$	$\mathrm{Var}^{(X)}$	$\Sigma^{(X)}$
-0.1	1.25	67.8725	4261.16	1.79940	34.2583	980.536	1.79498
	1.5	37.6737	1289.29	1.79576	19.0884	282.958	1.74084
	1.75	24.8236	554.508	1.78265	12.5632	117.937	1.60903
	2.0	18.1333	296.369	1.76089	9.10073	62.1734	1.49475
-0.15	1.25	66.9962	4051.36	1.80078	34.154	924.824	1.80030
	1.5	37.7258	1246.62	1.79625	19.441	271.907	1.72090
	1.75	25.1060	541.866	1.77518	12.9953	116.235	1.51999
	2.0	18.4684	292.267	1.73975	9.50499	63.4725	1.35219

Table 1: For the periodic input signal (13), $t_1^{(Y)}(y,\tau)$, $\mathrm{Var}^{(Y)}(y,\tau)$ and $\Sigma^{(Y)}(y,\tau)$ for $Y(t)$ are compared with $t_1^{(X)}(y,\tau)$, $\mathrm{Var}^{(X)}(y,\tau)$ and $\Sigma^{(X)}(y,\tau)$ for $X(t)$, respectively, with $\vartheta = 1$, $\mu = 0.1$, $\varrho = -0.9$, $\omega = 0.2$, $\phi = 5$, $B = -1$, $\tau = 0$, $y = -0.4$ and $S = 1.5$.

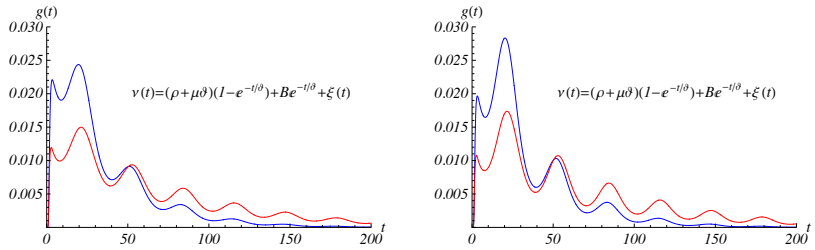

(a) $\sigma^2 = 1.25, \lambda = -0.1$ (b) $\sigma^2 = 1.25, \lambda = -0.15$

Figure 6: For the periodic signal (13), $g_Y(S,t|y,\tau)$ (red curve) and $g_X(S,t|y,\tau)$ (blue curve) are plotted for $\vartheta = 1$, $\mu = 0.1$, $\varrho = -0.9$, $\omega = 0.2$, $\phi = 5$, $\sigma^2(t) = \sigma^2(1 - e^{-2t/\vartheta})^2$, $B = -1$, $\tau = 0$, $y = -0.4$ and $S = 1.5$.

cillations having the same period Q of the periodic input signal. Hence, periodic subthreshold stimulation produces multimodal firing densities for noise intensities not too strong. The black curves in Figure 7 indicate the firing densities for the constant input signal $\mu(t) = \mu = 0.1$, in which the function $\xi(t) = 0$ in $\nu(t)$. We note that the firing densities $g_Y(S,t|y,0)$ and $g_X(S,t|y,0)$ oscillate around the related firing densities in the case of the constant input signal $\mu(t) = \mu$.

It should be emphasized that the behaviors of the firing densities of the unrestricted process $Y(t)$ subject to the periodic input signal (13) and a constant noise intensity are in agreement with those obtained in [2], [22], [25], [28], [30], for different choices of the parameters. Similarly, such behaviors occur also for the firing densities of the process $X(t)$ with reflecting boundary (19). In addition, as shown in Figures 4, 5 and 7 the first peaks of the firing densities are more pronounced for the process $X(t)$ than those of the firing density of $Y(t)$.

In Figure 8 we compare the firing densities of Figure 7 with the asymptotic exponential behaviors of the firing densities in the case of the constant signal $\mu(t) = \mu = 0.1$. As showed in [5], the dashed curves are the exponential densities

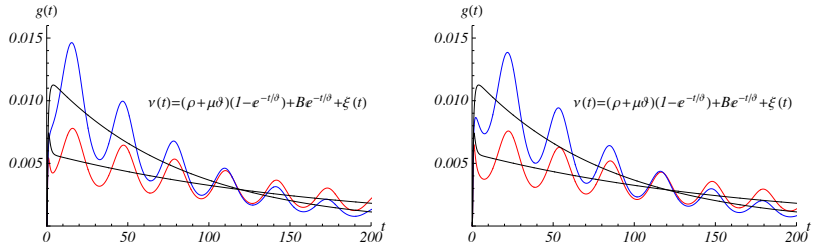

(a) $\phi = 0$ (b) $\phi = 5$

Figure 7: For the periodic signal (13), $g_Y(S, t|y, \tau)$ (red curve) and $g_X(S, t|y, \tau)$ (blue curve) are plotted for $\vartheta = 1$, $\mu = 0.1$, $\varrho = -0.9$, $\lambda = -0.1$, $\omega = 0.2$, $\sigma^2 = 1$, $B = -1$, $\tau = 0$, $y = -0.4$ and $S = 1.5$. The black curve indicate the firing densities for the constant signal $\mu(t) = \mu$.

$\gamma_X(t) = \alpha\, e^{-\alpha\, t}$ (blue curve) and $\gamma_Y(t) = (\alpha/2)\, e^{-(\alpha/2)\, t}$ (red curve), with

$$\alpha = \frac{2\,[S - (\varrho + \mu\,\vartheta)]}{\sigma\,\vartheta\,\sqrt{\pi\vartheta}}\,\exp\Big\{-\frac{[S - (\varrho + \mu\,\vartheta)]^2}{\sigma^2\,\vartheta}\Big\} \qquad (S > \varrho + \mu\,\vartheta). \tag{33}$$

Hence, denoting by $E(\widehat{T}_X^k)$ and by $E(\widehat{T}_Y^k)$ the moments of the exponential densities $\gamma_X(t)$ and $\gamma_Y(t)$, one has $E(\widehat{T}_X^k) = 2^{-k}\, E(\widehat{T}_Y^k)$ $(k = 1, 2, \ldots)$.

We remark that the exponential behaviors hold as the threshold S is progressively moved away from the starting point of the related processes.

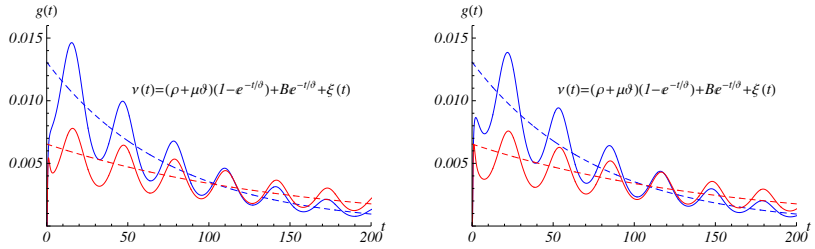

(a) $\phi = 0$ (b) $\phi = 5$

Figure 8: Same as in Figure 6. The dashed curves are the exponential density $\alpha\, e^{-\alpha t}$ (blue) and $(\alpha/2)\, e^{-(\alpha/2)t}$ (red), with α given in (33).

4.2. Asymptotic behavior of the firing pdf

For the process $X(t)$ with the transition pdf (9) and the periodic input signal $\mu(t)$ given in (13), we now analyze the asymptotic behavior of $g_X[S(t), t|y, \tau]$ when the intensity of the noise $\sigma^2(t)$ is a bounded $C^1(0, +\infty)$-class function, such that $\lim_{n\to+\infty} \sigma^2(t + n\,Q) = \widetilde{\sigma}^2(t)$, where $\widetilde{\sigma}^2(t)$ is a constant function or a periodic function of period $Q = 2\pi/\omega$.

Proposition 4.1. *Under the assumptions of Proposition 3.1, let $S(t)$ be a bounded $C^1(0,+\infty)$-class function, such that $\lim_{n\to+\infty} S(t+n\,Q) = \widetilde{S}$. Then,*

$$R_X(t) = -2 \lim_{n\to+\infty} \Psi_X\big[S(t+nQ), t+nQ|z,u\big] = \frac{2}{\widetilde{\sigma}(t)\,\vartheta\,\sqrt{\pi\vartheta}} \left\{ \widetilde{S} - (\varrho + \mu\,\vartheta) \right.$$
$$\left. - \frac{2\,\lambda\,\omega\,\vartheta^2}{1+\omega^2\vartheta^2}\,\sin(\omega\,t+\phi) - \frac{\lambda\,\vartheta\,(1-\omega^2\,\vartheta^2)}{1+\omega^2\vartheta^2}\,\cos(\omega\,t+\phi) \right\} \exp\Big\{ - \frac{\big[\widetilde{S} - \widetilde{M}(t)\big]^2}{\vartheta\,\widetilde{\sigma}^2(t)} \Big\}, \tag{34}$$

with Ψ_X defined in (11) and where $\widetilde{M}(t)$ is given in (16). Furthermore, if $\widetilde{S} > \varrho + \mu\vartheta + |\lambda|\,\vartheta/\sqrt{1+\omega^2\vartheta^2}$ one has $R_X(t) > 0$.

Proof. First of all, by setting $m_1(t) = m'(t)$, from (14) one has:

$$\lim_{n\to+\infty} m_1(t+n\,Q) = -\frac{\lambda\,\vartheta\,\omega}{1+\omega^2\vartheta^2} \Big\{ \sin(\omega\,t+\phi) - \omega\,\vartheta\,\cos(\omega\,t+\phi) \Big\}. \tag{35}$$

Then, making use of (16), (25), (27) and (35) in (11), one obtains (34). Since

$$\sup_{t\geq 0} \left[\frac{2\,\lambda\,\omega\,\vartheta^2}{1+\omega^2\vartheta^2}\,\sin(\omega\,t+\phi) + \frac{\lambda\,\vartheta\,(1-\omega^2\,\vartheta^2)}{1+\omega^2\vartheta^2}\,\cos(\omega\,t+\phi) \right] = \frac{|\lambda|\,\vartheta}{\sqrt{1+\omega^2\vartheta^2}},$$

one has:

$$\widetilde{S} - (\varrho + \mu\,\vartheta) - \frac{2\,\lambda\,\omega\,\vartheta^2}{1+\omega^2\vartheta^2}\,\sin(\omega\,t+\phi) - \frac{\lambda\,\vartheta\,(1-\omega^2\,\vartheta^2)}{1+\omega^2\vartheta^2}\,\cos(\omega\,t+\phi)$$
$$\geq \widetilde{S} - (\varrho + \mu\,\vartheta) - \frac{|\lambda|\,\vartheta}{\sqrt{1+\omega^2\vartheta^2}}; \tag{36}$$

hence, from (34) it follows that $R_X(t) > 0$ when $\widetilde{S} > \varrho + \mu\vartheta + |\lambda|\,\vartheta/\sqrt{1+\omega^2\vartheta^2}$. □

We note that the function $R_X(t)$, given in (34), is a periodic function with period $Q = 2\pi/\omega$, i.e. the same period of the input signal.

As the threshold $S(t)$ is progressively moved away from the starting point of the process $X(t)$, a non-homogeneous exponential approximation is shown to hold for the FPT pdf $g_X[S(t),t|y,\tau]$. Indeed, under the assumptions of Proposition 4.1, for $\widetilde{S} > \varrho + \mu\vartheta + |\lambda|\,\vartheta/\sqrt{1+\omega^2\vartheta^2}$, $g_X[S(t),t|y,\tau]$ admits the following non-homogeneous exponential asymptotic behavior:

$$g_X[S(t),t|y,\tau] \simeq R_X(t)\,\exp\Big\{ - \int_\tau^t R_X(\xi)\,d\xi \Big\} \equiv \widetilde{g}_X(t) \quad [\nu(\tau) \leq y < S(\tau)], \tag{37}$$

with $R_X(t)$ given in (34).

Moreover, we note that for the unrestricted process $Y(t)$, under the assumptions of Proposition 4.1, from (7) one has:

$$R_Y(t) = -2 \lim_{n\to+\infty} \Psi_Y\big[S(t+nQ), t+nQ|y,\tau\big] = \frac{R_X(t)}{2},$$

so that, starting from the integral equation (6), the FPT pdf $g_Y[S(t),t|y,\tau]$ admits the following asymptotic behavior:

$$g_Y[S(t),t|y,\tau] \simeq R_Y(t)\ \exp\left\{-\int_\tau^t R_Y(\xi)\,d\xi\right\} \equiv \widetilde{g}_Y(t) \qquad [y < S(\tau)]. \tag{38}$$

Results (37) and (38) can be obtained along the lines indicated in [12] and [23]. The agreement of the non-homogeneous exponential approximations (37) and (38) increases as the threshold is progressively moved away from the starting point of the related processes.

In Figure 9, by using the NIntegrate function in MATHEMATICA, we plot the asymptotic behaviors (37) and (38) of the firing densities $g_Y[S,t|y,\tau]$ and $g_X[S,t|y,\tau]$ for the same choices of parameters as in Figure 7. By comparing the

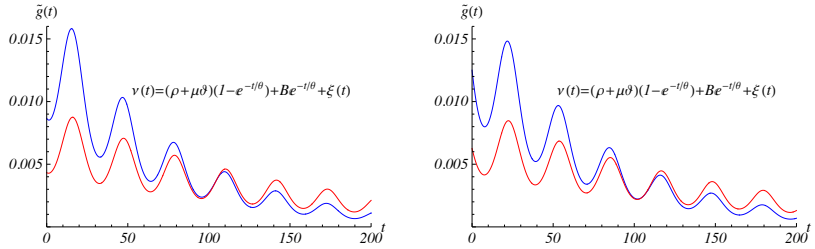

(a) $\phi = 0$ (b) $\phi = 5$

Figure 9: The asymptotic firing densities $\widetilde{g}_X(t)$ (blue curve) and $\widetilde{g}_Y(t)$ (red curve), given in (37) and (38) respectively, are plotted with the same choices of parameters of Figure 7.

numerical firing densities of Figure 8 with their related asymptotic behaviors (37) and (38) of Figure 9, we note that they differ only for small values of the time, after which a perfect agreement holds.

The k-order FPT moments of the asymptotic densities $\widetilde{g}_X(t)$ and $\widetilde{g}_Y(t)$, given in (37) and (38) respectively, are defined as:

$$\widetilde{t}_k^{(X)}(\tau) = \int_\tau^{+\infty} t^k\,\widetilde{g}_X(t)\,dt, \qquad \widetilde{t}_k^{(Y)}(\tau) = \int_\tau^{+\infty} t^k\,\widetilde{g}_Y(t)\,dt \qquad (k = 1,2,\ldots).$$

In Table 2 are reported the FPT asymptotic moments $\widetilde{t}_k^{(X)} \equiv \widetilde{t}_k^{(X)}(0)$ for $k = 1,2,3$, the coefficient of variation $\widetilde{\mathrm{CV}}^{(X)}$ and the skewness $\widetilde{\Sigma}^{(X)}$ for some choices of the period $Q = 2\pi/\omega = 8,4,2,1,0.5$. We note that the coefficient of variation is close to unity and the skewness tends to be close to 2 for decreasing values

of the period. Furthermore in the last three columns are indicated the ratios $r_k = \widetilde{t}_k^{(X)}/\widetilde{t}_k^{(Y)}$ for $k = 1, 2, 3$. We note that $r_k \simeq 2^{-k}$ $(k = 1, 2, 3)$, i.e. $\widetilde{t}_k^{(X)} \simeq 2^{-k}\,\widetilde{t}_k^{(Y)}$.

λ	ω	$\widetilde{t}_1^{(X)}$	$\widetilde{t}_2^{(X)}$	$\widetilde{t}_3^{(X)}$	$\widetilde{\mathrm{CV}}^{(X)}$	$\widetilde{\Sigma}^{(X)}$	r_1	r_2	r_3
-0.1	$\pi/4$	74.8130	11587.3	2.65×10^6	1.0345	1.7866	0.4942	0.2408	0.1313
	$\pi/2$	73.0744	11387.0	2.41×10^6	1.0642	1.8779	0.5024	0.2855	0.1227
	π	77.9606	11820.3	2.67×10^6	0.9720	1.9440	0.5036	0.2571	0.1260
	2π	77.2410	11695.2	2.65×10^6	0.9799	2.0137	0.5045	0.2531	0.1247
	4π	75.9052	11609.4	2.68×10^6	1.0075	2.0188	0.5002	0.2504	0.1258
-0.15	$\pi/4$	72.8273	11350.3	2.43×10^6	1.0677	1.6715	0.4775	0.2529	0.1307
	$\pi/2$	70.9035	11102.0	2.32×10^6	1.0993	1.6106	0.5070	0.2708	0.1264
	π	77.3175	11828.9	2.57×10^6	0.9893	1.7912	0.4974	0.2605	0.1314
	2π	76.4897	11796.0	2.76×10^6	1.0081	1.9215	0.5056	0.2572	0.1307
	4π	75.6436	11548.9	2.66×10^6	1.0091	2.0421	0.5016	0.2490	0.1257

Table 2: For the periodic input signal (13), $\widetilde{t}_k^{(X)}$ $(k = 1, 2, 3)$, $\widetilde{CV}^{(X)}$, $\widetilde{\Sigma}^{(X)}$, $r_k = \widetilde{t}_k^{(X)}/\widetilde{t}_k^{(Y)}$ $(k = 1, 2, 3)$ are reported with $\vartheta = 1$, $\mu = 0.1$, $\sigma^2 = 1$, $\varrho = -0.9$, $\phi = 0$, $B = -1$, $\tau = 0$, $y = -0.4$ and $S = 1.5$.

4.3. Simulations for the firing pdf

In order to simulate the firing pdf $g_X[S(t), t|y, \tau]$ through the threshold $S(t)$ we generate the sample paths of the Gauss-Markov process $Y(t)$ characterized by (2) and (14), from which the sample paths of the restricted process $X(t)$ are constructed taking in account the presence of the reflecting boundary $\nu(t)$ given in (19). By setting $t_0 = \tau$ and $Y(t_0) = X(t_0) = y$, we simulate $Y(t)$ at a discrete set of time points $t_1, t_2, \ldots$, such that $t_0 < t_1 < t_2 \ldots$ by using the stochastic recurrence equation (cf., for instance, [19]):

$$Y(t_k) = m(t_k) + \Big[Y(t_{k-1}) - m(t_{k-1})\Big] e^{-\Delta_k/\vartheta} + \xi_k \sqrt{\int_{t_{k-1}}^{t_k} \sigma^2(u)\, e^{-2(t_k-u)/\vartheta}\, du}, \qquad (k = 1, 2, \ldots), \tag{39}$$

where $m(t)$ is given in (14), $\Delta_k = t_k - t_{k-1}$ and $\xi_1, \xi_2, \ldots$ is a sequence of independent and identically distributed (*iid*) standard normal random variables. Hence, we set $X(t_k) = Y(t_k)$ if $Y(t_k) \geq \nu(t_k)$, elsewhere $X(t_k) = 2\,\nu(t_k) - Y(t_k)$ if $Y(t_k) < \nu(t_k)$. The simulation algorithm, described in more details in [5], provides a collection of N simulated first passage times of $X(t)$ through $S(t)$. Making use of the simulation algorithm, in Figure 10 the sample paths of the unrestricted process $Y(t)$ and of the restricted process $X(t)$ in the presence of the reflecting boundary (19) are represented for some choices of the parameters, with constant step $\Delta_k = 0.01$.

By means of the simulation algorithm, an estimation of the FPT pdf can be achieved by the histogram of the simulated first passage times. In Figure 11, the numerical firing density and the histogram of the simulated firing times, with constant step $\Delta_k = 10^{-4}$, are compared for the constant firing threshold $S = 1.5$.

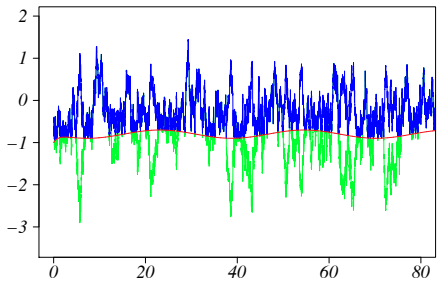

Figure 10: Sample paths of the unrestricted process $Y(t)$ (green) originating at $y = -0.4$ at time $\tau = 0$ with $\vartheta = 1$, $\mu = 0.1$, $\varrho = -0.9$, $\lambda = -0.1$, $\omega = 0.2$, $\phi = 5$, $\sigma^2 = 1$ and of the restricted process $X(t)$ (blue) in the presence of the reflecting boundary (19) with $B = -1$ (red).

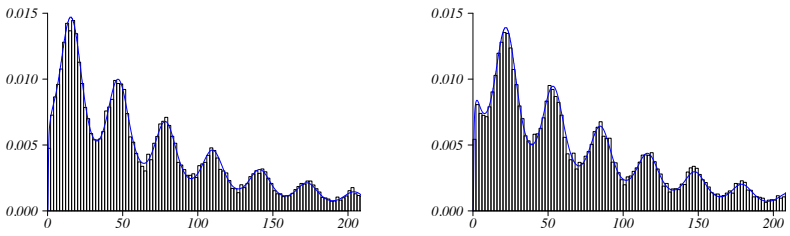

(a) $\phi = 0$ (b) $\phi = 5$

Figure 11: For the restricted Ornstein-Uhlenbeck process $X(t)$, the histogram of a sample of 30000 simulated firing times is compared with the numerical firing density $g_X(S, t|y, 0)$, obtained by (10), for $S = 1.5$ and the same choices of parameters of Figure 10.

5. Concluding remarks

In this paper we study the FPT problem for the inhomogeneous LIF model for single neurons activity in the presence of a lower reflecting boundary (19) and periodic input signals (13). The firing densities for the unrestricted LIF process $Y(t)$ defined in (5) with periodic input signals (13) and for the restricted LIF process $X(t)$, obtained from $Y(t)$ in the presence of the reflecting boundary $\nu(t)$ given in (19), are compared by using numerical, asymptotic and simulation procedures. In particular, the FPT densities of the unrestricted process $Y(t)$ and the restricted one $X(t)$ are compared with the same periodic input signals, given in (13), for constant threshold and constant intensity of noise. The influence of the noise intensity and of the amplitude of the periodic input signal is analyzed, showing that there are similar behaviors for the firing densities of the unrestricted process $Y(t)$ and of the restricted process $X(t)$. The peaks of the firing densities become more visible when the amplitude $|\lambda|$ of the input signal increases. When the intensity of the noise increases, the amplitude of the

input signal does not affect essentially in the shape of the firing densities. For low intensity of the noise, the peaks of the FPT pdf are spaced at multiples of the period of the input signal, except for the first few peaks; furthermore, the envelope of the peaks decays exponentially. Moreover, the first peaks of the firing densities are more pronounced for the process $X(t)$ than those of the firing density of $Y(t)$. However, the mean and the variance of FPT for the restricted process $X(t)$ are lower than those of the corresponding unrestricted process $Y(t)$. Under suitable assumptions on the noise intensity and on the threshold, the asymptotic behaviors of the firing densities for the unrestricted LIF process $Y(t)$ and for the restricted LIF process $X(t)$ are analyzed. Then, making use of such densities, the asymptotic FPT moments for the restricted LIF process $X(t)$ are evaluated for different choices of the period and of the amplitude of the signal; we note that the coefficient of variation is close to unity and the skewness tends to be close to 2 for decreasing values of the period.

We remark that the Volterra integral equation (10) can be useful in the parameters estimation of the restricted Ornstein-Uhlenbeck process in the presence of a periodic input signal. This topic will be developed in a future work in a similar way to what was done in [36].

Finally, the obtained results suggest the importance of the position of the lower boundary as well as that of the firing threshold when the statistical properties of LIF neuron models with periodic input signal (13) are investigated.

Acknowledgements This work has been performed under partial support of the G.N.C.S.- INdAM and Campania Region. We acknowledge the constructive criticism of anonymous reviewers on an earlier version of this paper.

References

[1] Benedetto E., Sacerdote L., Zucca C. (2013) A first passage time problem for a bivariate diffusion process: Numerical solution with an application to neuroscience when the process is Gauss-Markov. *Journal of Computation and Applied Mathematics* **242**, 41–52.

[2] Bulsara A.R., Elston T.C. Doering C.R, Lowen S.B., Lindenberg K. (1996) Cooperative behavior in periodically driven noisy integrate-fire models of neuronal dynamics. *Physical Review E 53*, no. 4, 3958–3969.

[3] Buonocore, A., Nobile, A.G. and Ricciardi, L.M. (1987) A new integral equation for the evaluation of first-passage-time probability densities. *Adv. Appl. Prob.* **19**, 784–800.

[4] Buonocore, A., Caputo, L. and Pirozzi, E. (2008) On the evaluation of firing densities for periodically driven neuron models. *Mathematical Biosciences* **214**, 122–133.

[5] Buonocore, A., Caputo, L., Nobile A.G. and Pirozzi, E. (2014) Gauss-Markov processes in the presence of a reflecting boundary and applications in neuronal models. *Appl. Math. Comput.*, **232**, 799–809 (Corrigendum: *Appl. Math. Comput.*, **241**, 11–12).

[6] Buonocore, A., Caputo, L. , Pirozzi, E., Ricciardi L.M. (2010) On a stochastic leaky integrate-and-fire neuronal model. *Neural Computation* **22**, 2258-2585.

[7] Burkitt, A.N. (2006) A review of the integrate-and-fire neuron model. II. Inhomogeneous synaptic input and network properties. *Biol. Cybernet.* **95** , no. 2, 97–112.

[8] Di Nardo, E., Nobile, A.G., Pirozzi, E. and Ricciardi, L.M. (2001) A computational approach to first-passage-time problems for Gauss-Markov processes. *Adv. Appl. Prob.* **33**, 453–482.

[9] Gammaitoni L., Hänggi P., Jung P., Marchesoni F. (1998) Stochastic resonance. *Reviews of Modern Physics* **70**, no. 1, 223–287.

[10] Gerstner, W. and Kistler, W.M. (2002). *Spiking neuron models: single neurons, populations, plasticity.* Cambridge University Press, Cambridge.

[11] Giorno, V., Nobile, A.G., Ricciardi, L.M. and Sato, S. (1989) On the evaluation of first-passage-time probability densities via non-singular integral equation. *Adv. Appl. Prob.* **21**, 20–36.

[12] Giorno V., Nobile A.G. and Ricciardi L.M. (1990) On the asymptotic behaviour of first–passage–time densities for one–dimensional diffusion processes and varying boundaries. *Adv. Appl. Prob.* **22**, 883–914.

[13] Giorno V. and Spina S. (2014) On the return process with refractoriness for a non-homogeneous Ornstein-Uhlenbeck neuronal model. *Mathematical Biosciences and Engineering* **11**, No. 2, 285–302.

[14] Giraudo, M.T. and Sacerdote, L. (2005) Effect of periodic stimulus on a neuronal diffusion model with signal-dependent noise. *BioSystems* **79**, 73–81.

[15] Inoue, J., Sato S. and Ricciardi L.M. (1997) A note on the moments of the first-passage time of the Ornstein-Uhlenbeck process with a reflecting boundary. *Ricerche di Mathematica*, Vol. XLVI, 87-99.

[16] Inoue, J. and Doi, S. (2007) Sensitive dependence of the coefficient of variation of interspike intervals on the lower boundary of membrane potential for leaky integrate-and.fire neuron model. *BioSystems* **87**, 49–57.

[17] Jahn, P., Berg, R.W., Hounsgaard, J. and Ditlevsen, S. (2011) Motoneuron membrane potentials follow a time inhomogeneous jump diffusion process. *J. Comput Neurosci* **31**, 563–579.

[18] Kobayashi, R., Shinomoto, S. and Lánský, P. (2011) Estimation of time-dependent input from neuronal membrane potential. *Neural Computation* **23**, 3070–3093.

[19] Kroese D.P., Taimre T., Botev Z.I. (2011) Handbook of Monte Carlo Methods. Wiley Series in Probability and Statistics. John Wiley & Sons, Hoboken, NJ.

[20] Lánský, P. (1997) Sources of periodical force in noisy integrate-and-fire models of neuronal dynamics. *Physical Review E* **55**, no. 2, 2040–2043.

[21] Lánský, P. and Ditlevsen, S. (2008) A review of the methods for signal estimation in stochastic diffusion leaky integrate-and-fire neuronal models. *Biol. Cybern.* **99**, 253–262.

[22] Longtin A. (1993) Stochastic Resonance in Neuron Models. Journal of Statistical Physics **70**, no. 1/2, 309–327.

[23] Nobile, A.G., Pirozzi, E. and Ricciardi, L.M. (2008) Asymptotics and evaluations of FPT densities through varying boundaries for Gauss-Markov processes. *Scientiae Mathematicae Japonicae* **67**, No. 2, 241–266.

[24] Pakdaman, K., Tanabe, S., Shimokawa T. (2001) Coherence resonance and discharge time reliability in neurons and neuronal models. *Neural Networks* **14**, 895–905.

[25] Plesser H.E. and Geisel T. (1999) Markov analysis of stochastic resonance in a periodically driven integrate-and-fire neuron. *Phys Rev E 59*, no. 6, 7008–7017.

[26] Ricciardi L.M. (1977) *Diffusion Processes and Related Topics in Biology*, Lecture Notes in Biomathematics, Vol. 14. Springer Verlag, Berlin.

[27] Ricciardi, L. and Lánský, P. (2003) Diffusion models of neuron activity. In: *The Handbook of Brian Theory and Neural Networks, Second Edition* (Arbib M.A, ed.), pp. 343–348, The MIT Press, Cambridge.

[28] Shimokawa, T., Pakdaman K. and Sato S. (1999) Time-scale matching in the response of a leaky integrate-and-fire neuron model to periodic stimulus with additive noise. *Physical Review E* **59**, no. 3, 3427–3443.

[29] Shimokawa, T., Pakdaman K. and Sato S. (1999) Mean discharge frequency locking in the response of a noisy neuron model to subthreshold periodic stimulation. *Physical Review E* **60**, no. 1, R33–R36.

[30] Shimokawa, T., Rogel A., Pakdaman K. and Sato S. (1999) Stochastic resonance and spike-timing precision in an ensemble of leaky integrate and fire neuron models. *Physical Review E* **59**, no. 3, 3461–3470.

[31] Shimokawa, T., Pakdaman K., Takahata T., Tanabe S. and Sato S. (2000) A first-passage-time analysis of the periodically forced noisy leaky integrate-and-fire model. Biol. Cybern. **83**, 327–340.

[32] Schindler, M., Talkner, P., Hänggi, P. (2005) Escape rates in periodically driven Markov processes. *Physica A*, **351**, 40–50.

[33] Tamborrino, M., Sacerdote, L., Jacobsen, M. (2014) Weak convergence of marked point processes generated by crossings of multivariate jump processes. Applications to neural network modeling. *Physica D*, **288**, 45–52.

[34] Touboul J. and Faugeras O. (2007) The spikes trains probability distributions: A stochastic calculus approach. *Journal of Physiology - Paris* **101**, 78–98.

[35] Tuckwell, H. C. (1988) *Introduction to theoretical neurobiology. Vol. 2. Nonlinear and stochastic theories*. Cambridge Studies in Mathematical Biology, Vol. 8. Cambridge University Press, Cambridge.

[36] Wonho Ha (2009) Applications of the reflected Ornstein-Uhlenbeck process. Doctoral Dissertation, University of Pittsburgh.